Modified Viologen- and Carbonylpyridinium-based Electrodes for Organic Batteries

Xiaoming He,[1,] Ling Chen,[1] Thomas Baumgartner[2,]**

*To whom correspondence should be addressed

[1] Key Laboratory of Applied Surface and Colloid Chemistry (Ministry of Education), School of Chemistry and Chemical Engineering, Shaanxi Normal University, Xi'an 710119, P.R. China

[2] Department of Chemistry, York University, 4700 Keele Street, Toronto, Ontario M3J 1P3, Canada

*Corresponding Author Email: xmhe@snnu.edu.cn, tbaumgar@yorku.ca

ABSTRACT. Efficient electrochemical energy storage has been identified as one of the most pressing needs for a sustainable-energy economy. Inorganic battery materials have traditionally been the center of attention, with the current state-of-the-art device being the lithium-ion battery. Recent pursuits have led to organic materials for their beneficial chemistry and properties, but suitable materials for organic batteries are still few and far between. This Spotlight on Applications highlights two intriguing pyridinium-based organic materials – modified viologens and carbonylpyridiniums that have both been successfully employed in electrode materials for solid-state Li-ion type organic batteries (LOBs). We will first provide an overview of the inherent electronic properties of each building block and how they can effectively be modified while maintaining or enhancing their desirable electrochemical properties for practical applications. We

then describe a range of different material designs for a battery context and their application in various organic device settings with some examples showing competitive performance with traditional Li-ion batteries.

Keywords. pyridinium, viologen, carbonylpyridinium, electrochemical energy storage, Li-ion batteries, organic batteries, organic electrodes

1. Introduction

Electrochemical energy storage has become one of the fastest growing research fields in recent years. The urgent need for more sustainable energy solutions such as solar and wind, and the concomitant reduction of hydrocarbon-based energy sources have led to rapidly accelerating activities around new and improved battery technologies.[1-4] Currently, state-of-the-art lithium-ion batteries (LIBs) represent the most widely employed technology,[5] but it is clear that this type of battery alone cannot satisfy the ever-growing and immediate demand for electrochemical energy storage solutions on large scales (i.e., for intermittent solar and wind energy), e-mobility (i.e., electrical vehicles, and hand-held electronic devices), as well as for other more specialized application areas. To this end, researchers worldwide are designing and developing a wide range of next-generation battery technologies beyond traditional Li-ion.[6,7] This includes leveraging other redox-active metal ions, such as sodium,[8] magnesium,[9] zinc,[10] and aluminum,[11] to name but a few, but also new types of electrode materials such as sulfur,[12] silicon,[13] and most notably organics.[14-17] Recent pursuits have led to organic materials for their beneficial light weight, low cost, and low environmental toxicity. However, to see competitive success, significant efforts are required to develop high energy-density organic electrodes based on novel materials capable of holding a large

number of charges and remaining stable until the release of that energy is desired. Finding the right balance between high charge-storage capacity, redox stability, (in)solubility, and efficient electrical conductivity for improved battery performance poses a formidable materials challenge, as highlighted throughout this Spotlight.

Current organic molecular architectures largely encompass a few main structural motifs, such as carbonyl/quinone and nitrogen-containing polyaromatic hydrocarbon building blocks[10] that show desirable electrochemical features and stabilities making them feasible and competitive materials for Li-ion type organic batteries (LOBs). *N*-alkylated pyridinium derivatives have become very attractive in this context due their to strong electron accepting properties.[28,29] Genuine *N*-methyl pyridinium exhibits irreversible redox properties that can be significantly improved by chemical modifications. The most popular strategy is the design of dimerized species, i.e., viologens (*N*,*N*'-alkylated-4,4'-bipyridylium salts) that show excellent reversible redox properties, along with intense color changes upon switching between their different redox states.[18-23] These features have received widespread attention in switchable electrochromic viologen materials.[24-27] Another emerging modified pyridinium species is carbonylpyridinium that occurs naturally in the NAD^+/NADH couple in the respiratory chain. By incorporation of a carbonyl group, particularly at the para-position of the pyridinium nitrogen atom, two reversible reduction processes can also be realized.[28,29] In this context, Sanford et al. have introduced the carbonylpyridinium scaffold as functional component for high-performance redox-flow batteries (RFBs);[30-34] the same is true for viologens, most notably through the work of Schubert.[35,36] In addition, recent pursuits in using these two building blocks for solid-state LOB applications have also been promising. The accomplishments thus far warrant a timely Spotlight on these materials and their application as electrode materials. Herein, we highlight modified viologens and carbonylpyridinium species, as

these systems have shown the most promise and versatility for the field. We will first talk about general features, chemical modification strategies and the resulting electrochemical properties of each building block, before discussing their application via different strategies and performance as battery electrodes.

2. Modification Strategies and Electrochemistry

N-Methyl pyridinium is an archetypical redox-active platform for accepting one electron, with a half-wave potential of *ca.* -1.30 V (*vs.* SCE).[37] However, the reduction of methylpyridinium on a Pt electrode was found to be an irreversible process due to the formation of the "tail-to-tail" dimer, methyl viologen (**MV**$^{2+}$) (Figure 1). Compared to *N*-methyl pyridinium, **MV**$^{2+}$ is a stronger electron acceptor, and exhibits two reversible electron-transfer waves at -1.09 and -1.52 V (*vs.* Fc^+/Fc)[18] or -0.45 V and -0.76 V (*vs.* NHE). Due to the strongly electron-withdrawing pyridinium group, the direct connection of the two pyridinium rings substantially lowers the reduction threshold of the adjacent pyridinium unit. Once one of the pyridinium units is reduced, it effectively behaves as an electron-donating group toward its adjacent group, and therefore the second electron transfer inevitably occurs at a distinctly higher (negative) potential.

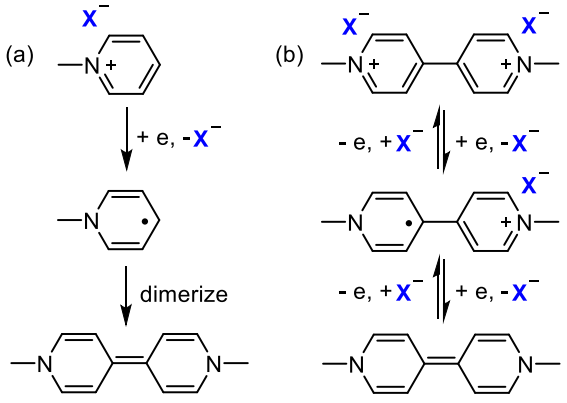

Figure 1. Reduction process of (a) methylpyridinium and (b) **MV**$^{2+}$.

The redox properties of viologens and pyridiniums are directly related to their chemical structure. Over the last two decades, a diverse set of modified viologens has been designed to tailor their redox potentials. In this part, we will summarize some of the typical strategies and state-of-the-art structures of modified viologens and methylpyridiniums and discuss how their redox properties are influenced (and potentially improved for use as battery electrode materials). Generally speaking, the electrochemical properties of these species can be effectively tuned via four strategies (Figure 2): i) Fused viologens: introduction of bridging main group elements between the two rings of bipyridine; ii) Core-extended viologens: introduction of rigid, conjugated linkers between the two pyridine units; iii) N-arylated viologens: introduction of aromatic moieties directly on one or both bipyridine nitrogen atoms; and iv) carbonylpyridiniums: introduction of carbonyl groups to the pyridinium skeleton.

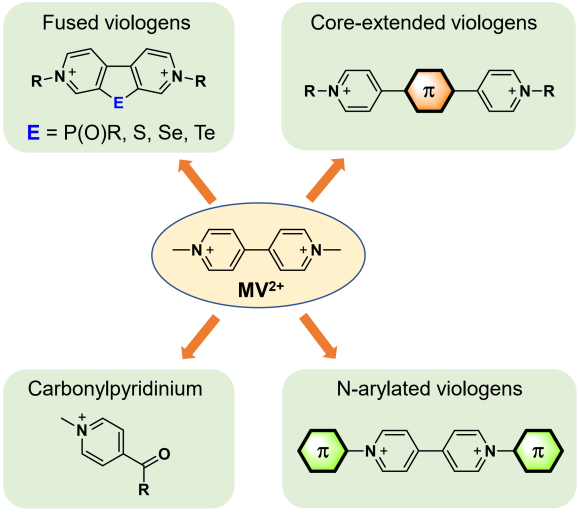

Figure 2. Four approaches toward modified viologens and carbonylpyridinium species.

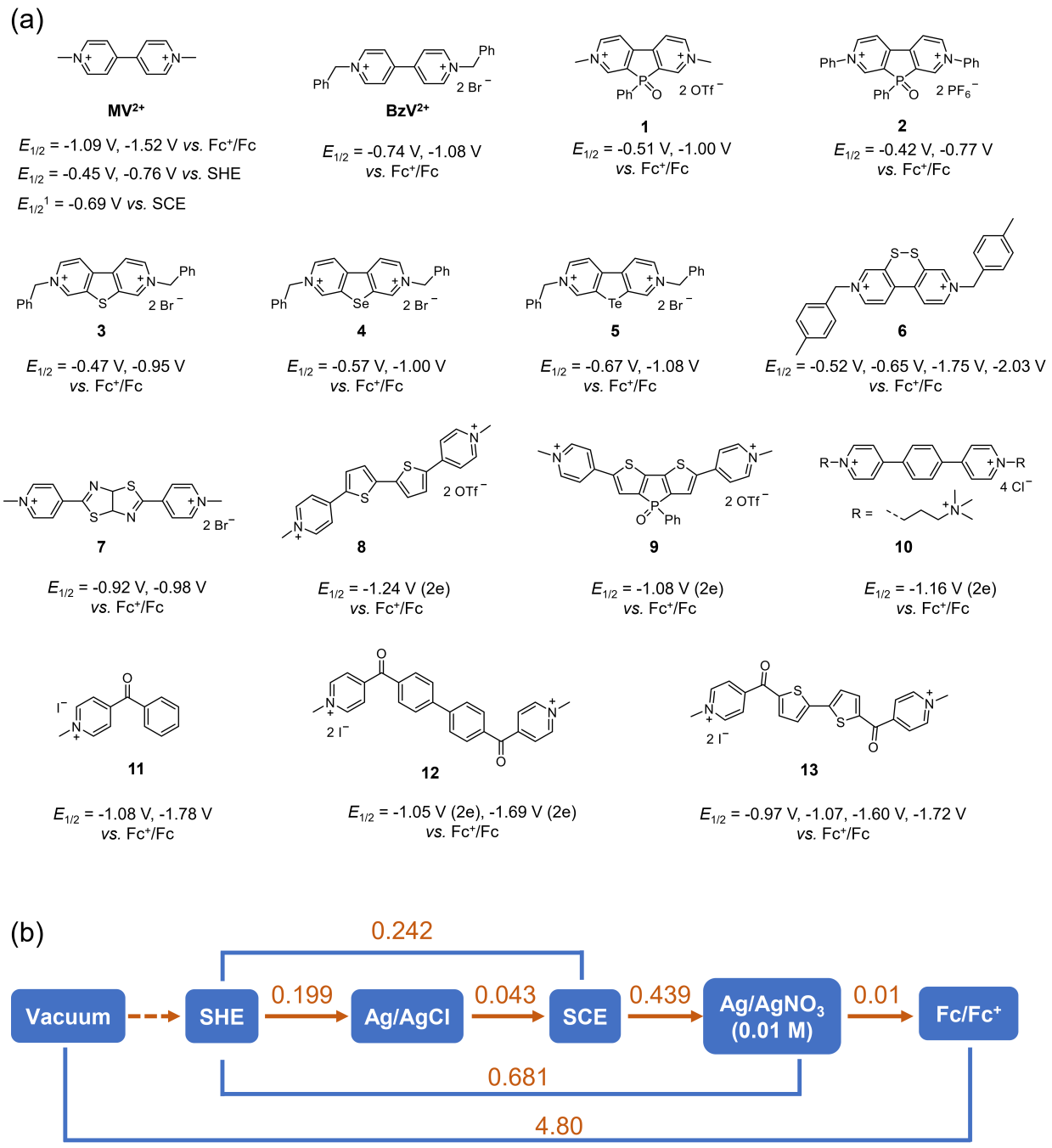

Figure 3. (a) Structures and redox potentials of representative modified viologens and methyl pyridiniums. (b) Redox potentials in [V] for different reference electrodes *vs*. vacuum.

Representative structures and redox potentials are summarized in Figure 3a. It should be noted in this context that redox potential values are often found based on different reference electrodes in the literature, such as Ag/Ag^+ ($Ag/AgNO_3$), Ag/AgCl, Fc^+/Fc (ferrocene), SCE (saturated calomel electrode), or SHE (standard hydrogen electrode), making a direct correlation of their redox properties less straightforward. For better comparison, we have listed the redox potentials of each species against Fc^+/Fc in Figure 3a as well and provide pertinent reference electrodes in Figure 3b. But it is important to note that the precise comparison of these reduction potentials also requires the consideration of solvent polarity, counter anions, electrolyte, scan rates, and so on. For that reason, we also refer to the potentials in the discussion as they were reported in the original literature.

2.1 Fused viologens. The bridging of bipyridine with main group elements (i.e., P(O)R, S, Se, and Te) is a very effective strategy for altering the electrochemical properties by increased planarity of the system and the donor/acceptor properties of the bridging atoms.[38] This class of viologens typically gives two clear stepwise, one-electron transfer processes due to the strong electronic communication between two pyridinium rings, similar to the cyclic voltammetry (CV) profile of $\mathbf{MV^{2+}}$. When the bridging atom is a strong electron acceptor, such as phosphoryl oxide group in **1**, the modified viologen exhibits much stronger electron-accepting properties. Both reduction potentials of **1** ($E_{red1/2}$ = -0.51 V and -1.00 V, *vs.* Fc^+/Fc) are significantly lower than the parent $\mathbf{MV}^{2+}$ ($E_{red1/2}$ = -1.09 V and -1.52 V, *vs.* Fc^+/Fc).[39] Such strong electron-accepting character of the phosphaviologen scaffold allows the utilization of both redox steps in a battery setting (as opposed to the parent $\mathbf{MV}^{2+}$) doubling the electron capacity per molecule (*vide infra*). Moreover, the stronger electron-acceptor properties of the modified viologens also increase the battery voltage with respect to the Li/Li^+ couple when used as a cathode, which potentially translates to more

powerful battery performance. These species are thus deemed superior electrode materials to the conventional non-bridged viologens. On the other hand, when the bridging atoms have electron-donor character, such as S, Se, Te, the resulting chalcogen-viologens exhibit a more facile first-electron uptake, when comparing **3** (-0.47 V *vs.* Fc^+/Fc), **4** (-0.57 V *vs.* Fc^+/Fc), **5** (-0.67 V *vs.* Fc^+/Fc), and $\mathbf{Bz_2V^{2+}}$(-0.74 V *vs.* Fc^+/Fc).[40] Benniston et al. have demonstrated that incorporation of a disulfur (S-S) bridge into the viologen scaffold leads to a storage capability of up to four electrons (Figure 4) in **6**, due to the contributions from the viologen skeleton and the reducible S-S bond.[41] The first two one-electron reductions, occurring at $E_{1/2}$ = -0.03 V and -0.16 V (*vs.* Ag/AgCl; -0.52 and -0.65 V *vs.* Fc^+/Fc), come from the viologen skeleton. This is then followed by breaking of the disulfide bridge, with the reductions at $E_{1/2}$ = -1.26 V and -1.54 (*vs.* Ag/AgCl; -1.75 and -2.03 V *vs.* Fc^+/Fc), respectively.

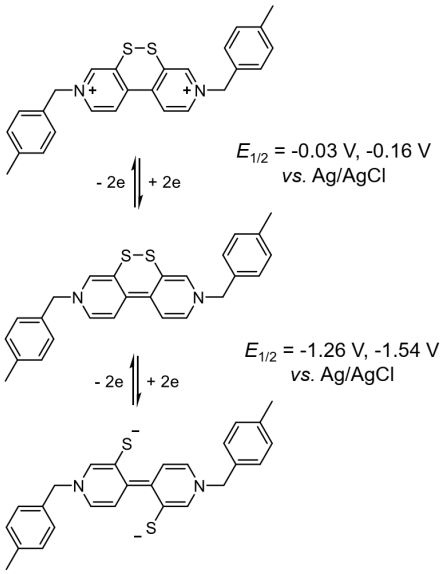

Figure 4. Four reduction processes of **6**.

2.2 Core-extended viologens. The introduction of a bridging conjugated planar linker helps to alleviate or prevent the communication between the two pyridinium redox centers, generally

resulting in closely spaced reduction peaks or overlapping two-electron storage behavior.[42,43] For instance, molecule **7** with the extended bispyridinium with thiazolo[5,4-d]thiazole (TTz) core, shows two reversible, closely spaced reduction peaks at -0.52 and -0.58 V (*vs.* SCE; -0.92 and -0.98 V *vs.* Fc^+/Fc).[42] Consequently, the potential gap between the two-step, one-electron transfer processes is narrowed to 60 mV, compared with the 310 mV for $\mathbf{MV^{2+}}$. Probably due to the less bulky fused five-membered ring of TTz, **7** still provides a slight electronic communication between the pyridinium rings, and therefore displaying two distinguishable steps during reduction. We were able to confirm that using a bithienylene core in **8** fully disrupts the communication, leading to a single two-electron reduction event at -0.75 V (*vs.* Ag/AgCl; -1.24 V *vs.* Fc^+/Fc).[44] Notably the concomitant fusion of the core with a phosphoryl group in **9** significantly lowers the reduction threshold (-0.59 V *vs.* Ag/AgCl; -1.08 V *vs.* Fc^+/Fc), while maintaining the reversible single two-electron nature of the reduction event. Similarly, by inserting a 1,4-phenylene spacer, such as in **10**, the electronic interaction between two pyridinium rings is also effectively blocked, leading to independent behavior of the two rings during the reduction process, yielding one two-electron transfer wave.[45] The electrons in the highly reduced viologen **10** are then delocalized over an extended range and maintain the structural stability of the scaffold that is beneficial for improving cycling stability in a battery setting. In addition, such overlapping two-electron storage may provide uniform plateaus in organic batteries and prevent significant energy loss in the form of heat (*vide infra*).

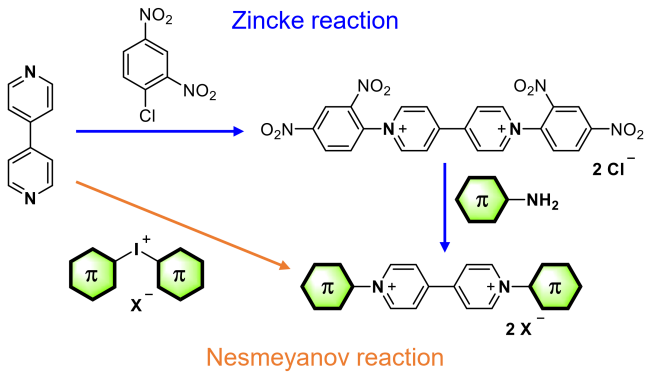

Figure 5. Two general strategies for the preparation of N-arylated viologens.

2.3 *N*-Arylation. As valuable complementary strategy to core-extension, *N*-arylation also provides an effective way to further extend the overall π-system of the core, allowing to tune the electrochemical properties more efficiently. Most synthetic approaches rely on the Zincke reaction (Figure 5)[46] that involves the pre-activation of pyridines by S_NAr reaction with the strongly electron-deficient 2,4-dinitrochlorobenzene (**DNCB**) to afford the *N*-arylated pyridinium (Zincke) salts. Further treatment with primary-amine-substituted aromatics/heteroaromatics leads to the formation of *N*-arylated viologens. Recent work by us has demonstrated Cu(II)-catalyzed Nesmeyanov reaction is an very effective protocol to prepare *N*-arylated viologens with electron-deficient phosphaviologen core (e.g., **2**) that are impossible to synthesize otherwise.[25] The *N*-arylation can significantly lower the LUMO energy, thus leading to easier electron injection. For example, both reduction potentials of **2** ($E_{1/2}$ = -0.42 V and -0.77 V, *vs.* Fc^+/Fc) are noticeably lower than those of **1** ($E_{1/2}$ = - 0.51 V and -1.00 V, *vs.* Fc^+/Fc) and the direct result of the peripheral π-extension of the scaffold.

2.4 Carbonylpyridinium. The carbonylpyridinium moiety is a key motif in the naturally occurring NAD^+/NADH cofactor that functions as an electron-transfer catalyst in the respiratory chain. When compared to the parent *N*-methyl pyridinium, incorporation of a carbonyl group

significantly improves the electrochemistry of the system. As early as 2001, Leventis et al. reported a series of 4-benzoyl-*N*-methylpyridinium (**BMP**) derivatives and investigated their electrochemistry.[28,29] This skeleton merges key features of viologens and quinones, and it can reversibly accept two electrons (Figure 6). The two reduction processes transform the cationic skeleton to a neutral radical species, and further to an anionic species, on a relatively low molecular weight entity (which is beneficial for high energy density in a battery). The use of acylpyridinium derivatives has been proven to be highly promising for redox-flow batteries by Sanford and coworkers.[30-34] In a related context, our group has recently developed a series of carbonylpyridinium polymers for LOBs (*vide infra*).

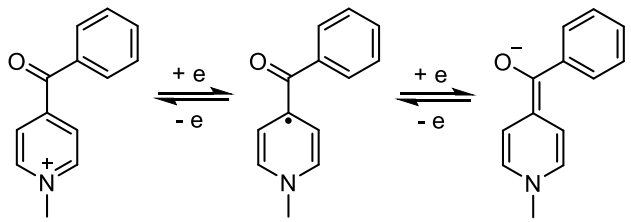

Figure 6. Two reduction processes of **BMP**.

3. Viologen-based Electrodes for Li-ion Batteries

Due to their well-defined redox behavior and ease of modification, viologens have been employed as battery electrodes in a variety of forms, including small molecules as well as polymers. The research focuses on their general utility, but also on alleviating performance issues in a LOB device setting by considering the electrochemical interfaces, as well as the long-term stability of the assembled electrode, vis-à-vis the (in)solubility of the electrode materials in the electrolyte solution. In theory, the performance of electrode materials, such as theoretical capacity, redox potential, kinetics and cycling stability, is essentially determined by their molecular structures. Specifically, the capacity depends on the molecular weight and the number of electrons transferred

during the redox reaction. The output voltage of a battery is the potential gap between the cathode and anode. One of the challenges for viologen-based active materials is the unwanted dissolution in nonaqueous liquid electrolyte, which will lead to poor cycling stability. Despite the pristine charged states have great advantage in suppressing the solubility in many organic electrolytes, their reduced species typically tend to have higher solubility. To this end, viologens have been modified via their *N*-alkyl substituents toward small molecule-based functional materials, or by incorporation into polymeric systems via *N*-alkylation or -arylation (Figure 7). The following discusses some representative examples and approaches.

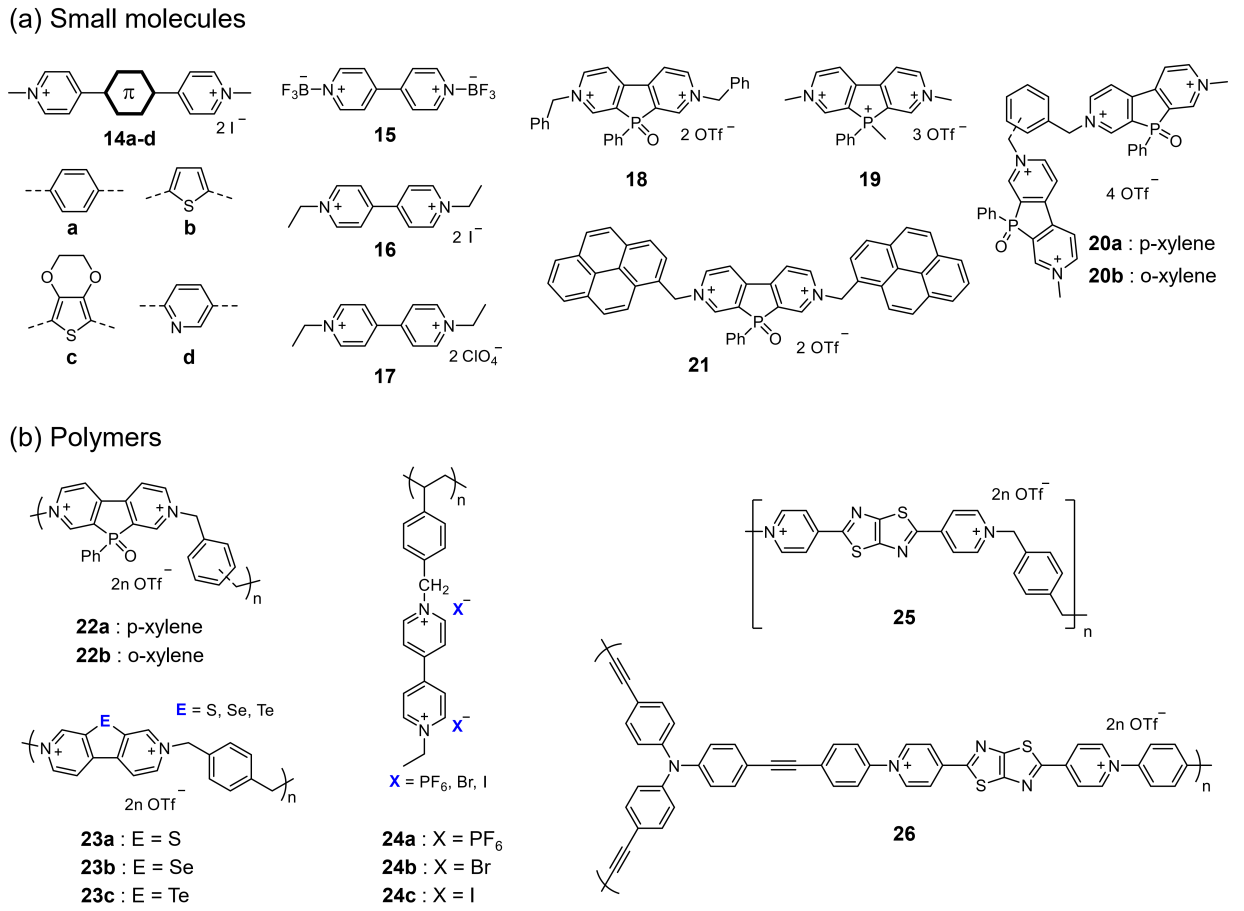

Figure 7. Representative viologen-based small molecules (a) and polymers (b) for organic solid-state LOBs.

3.1 Small molecules. The use of the π-extended viologen derivatives **14a-d** in LOBs has been reported by Yao and coworkers (Figure 7).[47] These derivatives show average voltages of approximately 2 V (*vs.* Li^+/Li), which is lower than that of conventional viologen derivatives. Unfortunately, the battery performance suffers from poor cycling stability, as a result of the dissolution of the active materials into the electrolyte solution during cycling, highlighting one of the major application challenges for small-molecule electroactive materials. Among these four compounds, the benzene-inserted derivative **14a** delivered a maximum anodic capacity of 70 mAh/g, which decreased to 38 mAh/g after 10 cycles. A recent report has shown that the complexation of BF_3 to the nitrogen atoms of 4,4'-bipyridine to from zwitterionic acceptor **15** (Figure 7)[48] affords a capacity of 175 mAh/g at 50 mAh/g, close to its theoretical capacity of 183 mAh/g; however, an obvious capacity decay was observed during the cycling. Compared to **14a-d**, the cycling performance of **15** was found to be improved, probably because the reduced species can still maintain a 'salty state' to suppress the dissolution.

Organic ionic crystals represent an attractive class of active materials for rechargeable batteries owing to their low solubility in common battery electrolytes, thereby inherently enhancing the stability of the electrode/electrolyte interface. Ma et al. studied ionic crystals of ethyl viologen (EV) with redox-active I^- (**16** or **EVI_2**), and non-redox-active (inert) ClO_4^- anions (**17** or **$EV(ClO_4)_2$**) as cathode materials for Li-ion batteries (Figure 8).[49] **EVI_2** and **$EV(ClO_4)_2$** display similar monoclinic systems in the solid state, with alternating organic EV^{2+} layers and inorganic I^-/ClO_4^- layers and their charge/discharge curves, capacities and rate performances are clearly anion-dependent. The **EVI_2** electrode exhibited a high initial discharge plateau at 3.7 V (*vs.* Li^+/Li) and delivered high device capacity because of the involvement of the redox-active I^- in the

energy-storage process. The reversible capacity of the **EVI_2** electrodes decreased slightly from 230 mAh/g to 210 mAh/g as the current rate increased from 0.1 C to 2 C. Even at a very high rate of 5 C, the **EVI_2** electrodes delivered a quite high capacity of 149 mAh/g, which corresponds to a capacity retention of about 65%. When I^- is replaced by the redox-inert ClO_4^-, the obtained **$EV(ClO_4)_2$** electrode displays lower capacity. However, benefiting from the good electron conduction of the ClO_4^- layers, **$EV(ClO_4)_2$** exhibits an excellent rate performance; even at 5 C, a high capacity of 102 mAh/g could be retained, which corresponds to 78% of the value at 0.1 C. Both compounds also show excellent cycling stability, with capacity retentions of 96% and 98% for **EVI_2** and **$EV(ClO_4)_2$** after 200 cycles, highlighting that using crystalline nanostructures of small organic molecules is an effective strategy to enhance cycling stability and performance.

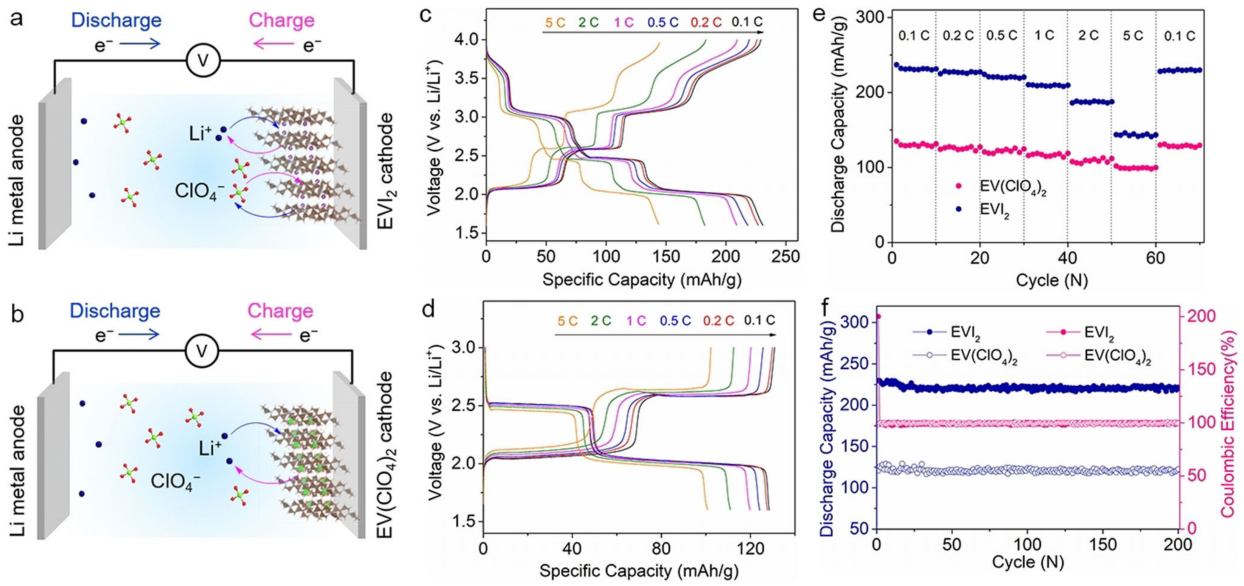

Figure 8. Schematic diagrams of a) **EVI_2** and b) **$EV(ClO_4)_2$**-based lithium batteries. Voltage profiles of the c) **EVI_2**- and d) **$EV(ClO_4)_2$**-based lithium batteries at various rates from 0.1 C to 5 C. e) Rate cyclability of the **EVI_2**- and **$EV(ClO_4)_2$**-based lithium batteries at various rates from 0.1 C to 5 C. f) Cycling stability and Coulombic efficiency of the **EVI_2**- and **$EV(ClO_4)_2$**-based lithium batteries at 0.5 C. Reproduced with permission from Wiley, ref. 49.

Our own pursuits into small-molecule-based organic electrodes involved the phosphaviologen system that we had originally introduced in 2011[39] and successfully employed in electrochromic applications in 2015 before.[24,25] Due to the significantly lowered reduction threshold compared to the parent $\mathbf{MV^{2+}}$ (*vide supra*), we were able to utilize both reduction events for **1** and **18** in a battery setting, resulting in theoretical specific capacities of 88 and 71 mAh/g, respectively.[50] In 2020, we then leveraged the modification of the phosphorus center toward the tricationic species **19** capable of reversibly storing three electrons, which translates into an impressive theoretical specific capacity of 262 mAh/g (when excluding the counter anions).[51] However, while the coulombic efficiencies were found to be high (>90%), all of species exhibited a rapid decay of their specific capacities down to only about 25% of their theoretical values after only a few charge/discharge cycles. This was attributed to an increasing solubility of the reduced (and less polar) states of the phosphaviologens in the electrolyte, leading the active electrode materials to leach into the electrolyte solution. Incorporation into oligomeric species with two phosphaviologen units (**20a-b**) did not remedy the dissolution of the active species from the electrode either.[50] To overcome the electrode-interface stability issue, we then modified the phosphaviologen core with pyrene-containing *N*-alkyl groups (**21**), capable of π-stacking with the conductive single-wall carbon nanotube-based (SWCNT) additive in the electrode.[52] While the larger molecular weight of **21** reduces the overall theoretical specific capacity to 53 mAh/g, this strategy nonetheless provides a sufficiently strong interface, with the active species showing excellent performance over up to 500 charge/discharge cycles at 1 C, without noticeable decay in capacity and an outstanding coulombic efficiency near 100%. Notably, the battery also performed at a high voltage between 1.95 and 3.5 V (*vs.* Li/Li^+) (Figure 9).

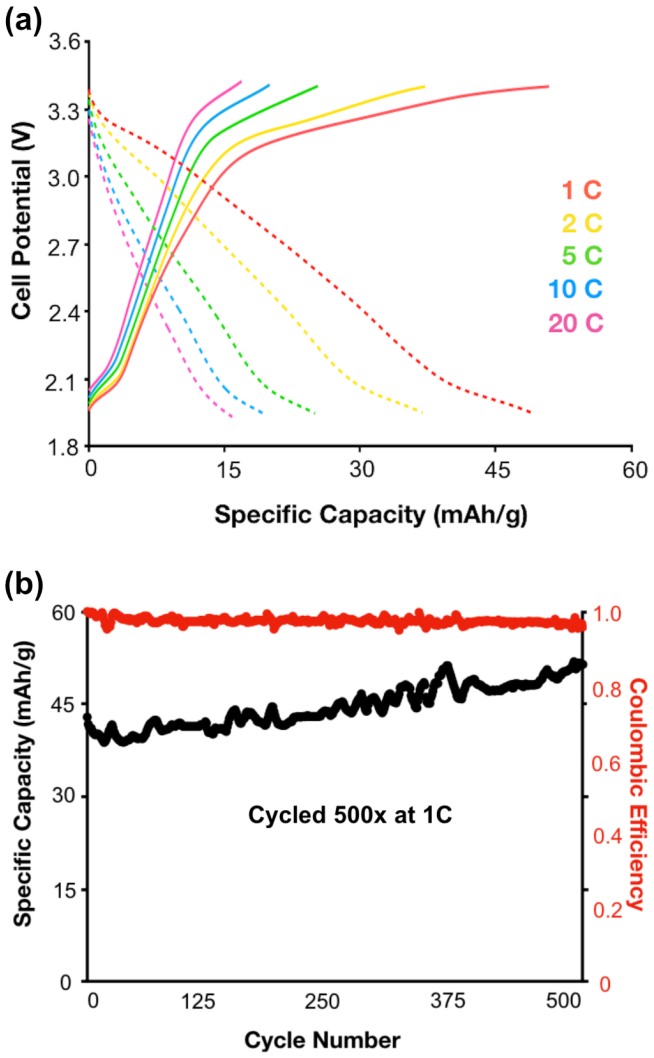

Figure 9. a) Charge-discharge profiles at varying C-rates for Li-ion batteries (coin-cell) fabricated using **21**:SWCNT composites as the cathode. b) Cycling stability for a **21**:SWCNT composite at 1 C. After 500 cycles the battery capacity slightly improves to 50 mAh/g, corresponding to 94 % of its theoretical capacity, and maintains a high coulombic efficiency throughout the experiment. Reproduced with permission from Wiley, ref. 52.

3.2 Polymers. To overcome the observed issues with the dissolution of small-molecule active materials from the organic electrodes as a function of their redox state/varied polarity, researchers often rely on a polymer approach. Polymers can commonly bind more strongly with the other

material components of the electrode composite, thereby leading to a sturdier interface with the electrolyte. However, the challenges here lie within the effective incorporation of the electroactive units, without compromising their energy-storage abilities. Conjugated systems can be detrimental in this regard, as communication between the redox-active units is enhanced in these systems, which considerably reduces the electron-storage capacity of the electrode. Conveniently, viologens and their reactivity can be effectively leveraged in this regard by using suitable *N*-alkyl substituents.

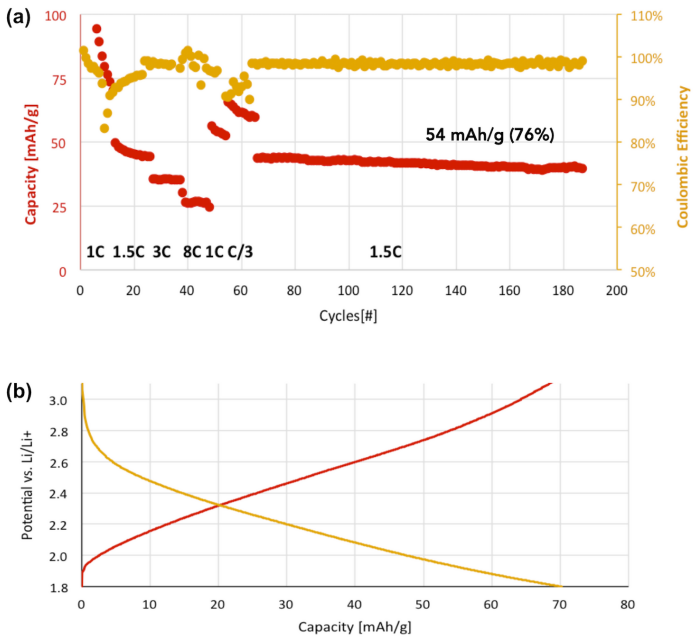

Figure 10. a) Half-cell cycling of **22b**, yellow dots correspond to coulombic efficiency and red dots correspond to capacity; b) Charging/discharging profile of **22b**. Adapted with permission from Wiley, ref. 50.

We have used the polymer approach for the phosphaviologen system, after the small-molecule versions of the materials were found to dissolve in the electrolyte during battery operation and continued charge/discharge cycling. To our satisfaction, polymers **22a-b** with *ortho*- and *para*-xylylene linkages, respectively, were found to be considerably more stable that their molecular congeners, with the specific capacities stabilizing around 50-60 mAh/g during repeated

cycling at 1 C, corresponding to roughly 76%-82% of the theoretical capacity for the species (Figure 10).[50] As already observed for the small-molecule materials, both polymers exhibited outstanding coulombic efficiencies near 100%, even after 150 charge/discharge cycles, and performed at an impressive voltage range from 1.8 to 3.1 V (*vs.* Li/Li^+), depending on their state of charge.

Similarly, Li et al. recently studied a series of stable poly(chalcogenoviologen)s **23a-c** with multiple and reversible redox events as anodes for high-performance organic Li-ion batteries (Figure 7).[40] Incorporation of heavy chalcogen atoms from S via Se to Te reduces the HOMO–LUMO gap, resulting in increased electron density and improved electrical conductivity. Such trends are also reflected in the battery performance **23a** < **23b** < **23c**. Reversible discharge capacities of 416, 462 and 502 mAh/g at 100 mA/g were achieved for **23a**, **23b** and **23c**, respectively. The best experimental capacity of Te-based **23c** was attributed to the increased electric conductivity and "superlithiation" processes on the Te-based material (Figure 11).

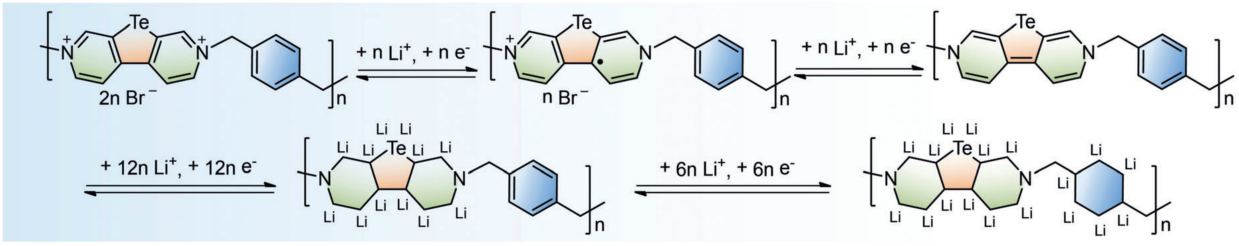

Figure 11. Proposed electrochemical reduction steps of **23c**. Reproduced with permission from Wiley, ref. 40.

Wang et al. reported a series of viologen-based cationic polymers **24a-c** with different counter anions (PF_6^-, Br^- or I^-), and evaluated their electrochemical performance as cathodes for LOBs (Figure 12).[53] In contrast to the electrochemically inert PF_6^- counter anion, the halides (Br^- or I^-)

are redox-active and can also participate in the energy-storage process. Besides the two characteristic redox couples from the viologen skeleton, **24b** (or PVBVEtBr$_2$) displays another strong and reversible redox peak at 3.53 V coming from the Br^-/Br_3^- redox couple; and **24c** (or PVBVEtI$_2$) exhibits two redox peaks centered at 3.12 and 3.66 V corresponding to oxidation of I^- to I_3^- (3.12 V) and then to I_2 (3.66 V). Benefitting from the participation of the halide redox couples, these two poly(viologen halide) electrodes lead to high discharge voltages up to 3.7 V (*vs.* Li/Li^+). At 0.02 A/g, **24b** and **24c** electrodes show excellent capacity of 186 and 185 mAh/g, respectively, much higher than **24a** (108 mAh/g). When using carbon cloth as a current collector, the **24c** cathode (with high mass loading of 80 wt%) presents improved cycling stability (89% capacity retention after 600 cycles at 0.1 A/g) and rate performance (110 mAh/g at 2 A/g). The same group also demonstrated halogen anion-dependent LOBs using viologen-based ionic porous polymers.[54] The utilization of a porous structure, offers excellent long-term cycling stability.

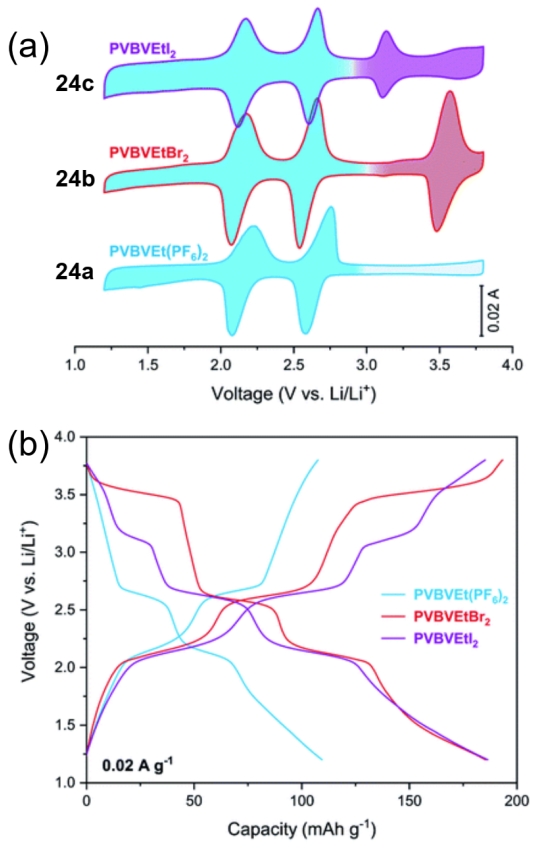

Figure 12. (a) CV curves at 0.1 mV/s and (b) initial charge/ discharge curves at 0.02 A/g of **24a-c**. Reproduced with permission from RSC, ref. 53.

Apart from the molecular design, morphology engineering has also been an effective strategy to boost the electrochemical properties of electrode materials, yet it is still a great challenge and has largely been unexplored.[55,56] In a recent contribution, our group reported a fibrous conjugated microporous polymer **26** by synergistic polymerization and self-assembly (Figure 13).[57] Compared to the linear polymer **25** with bulky morphology, the nanostructured morphology of **26** can significantly boost the ion and electron transport, and yields excellent LOB performance. Its Na^+ diffusion coefficient (D_{Li^+}) value is about 6.7 times larger than that of the linear counterpart. Moreover, **26** shows a significantly smaller charge-transport resistance (R_{ct}) of

77.22 Ω, compared to 210.80 Ω for **25**. At a high current density of 800 mA/g, the fibrous electrode can maintain a high capacity of 358.8 mAh/g after 1000 cycles, and the capacity retention rate is close to 100%. This excellent battery performance is far superior to those of the parent state-of-the-art viologen materials.

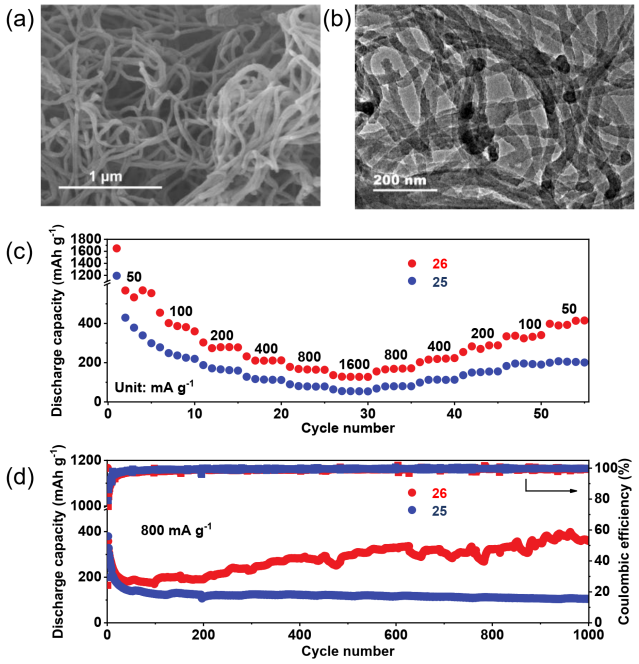

Figure 13. (a) SEM and (b) TEM of **26**, (c) rate performance and (d) long-term cycling properties at 800 mA g^{-1} for **25** and **26**. Reproduced with permission from RSC, ref. 57.

Rodríguez-Lopez and coworkers reported a promising class of viologen-containing redox active colloids (RACs) via post-polymerization of ethylviologen and colloidal cross-linked poly(vinylbenzyl chloride) particles (Figure 14).[58] The size of the well-defined 3D geometry can be readily tuned by selection of the desired colloid precursors. The large dimensions show promise in size-exclusion RFBs by greatly reducing crossover, while preserving the redox properties of their small-molecule constituents. The synthetic versatility may open new avenues for preparation

of pyridinium- and viologen-containing redox active colloids and inspire further research in solid-state batteries.

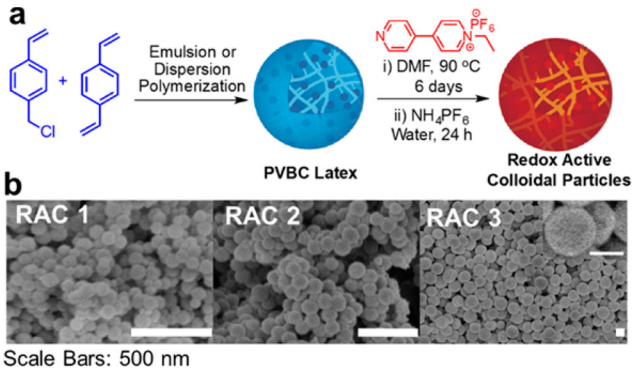

Figure 14. Synthesis and SEM images of redox-active colloidal particles (RACs). (a) Reaction scheme for the synthesis of polyvinyl benzyl chloride and viologen-based redox-active colloidal particles. (b) SEM images of viologen RACs with different particle diameters (80 ± 11, 135 ± 12, and 827 ± 71 nm).[64]

3.3 Anion shuttle batteries. Viologens have a positive molecular skeleton that is accompanied by various anions. Apart from tuning the structure of redox-active viologens, the counter anions have been demonstrated to play important role on the battery performance as well. In compounds **16** and **24**, for example, the Br^- and I^- counter anions are also redox-active and provide an additional capacity contribution. On the other hand, the electrochemical storage mechanisms of viologens involve the anion release and uptake (Figure 1). When using viologen electrodes for metal-ion batteries, the electrolyte anions reversibly shuttle to/from the cathode during charge/discharge, a system referred to as "anionic rocking-chair cell". This is quite different from many other n-type cathodes, such as quinones, that only involve metal-ion shuttle during charge and discharge. Such anionic rocking-chair cell configuration helps promote the fabrication of molecular (metal-free) rechargeable batteries, which potentially solves the problem of lithium dendrite formation. In

addition, the anions are poorly solvated in the polar electrolyte media due to their low solvation Gibbs energy, which facilitates the ion transfer into the electroactive materials.

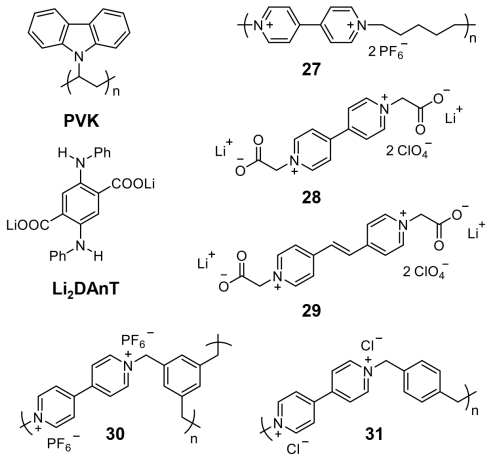

Figure 15. Chemical structures of viologens used in anion shuttle batteries.

This unconventional cell configuration based on viologens was first explored by Yao and co-workers who designed a rocking-chair type molecular ion battery with PF_6^- as the charge carrier, by assembling poly(1,5-pentylene-4,4'-bipyridinium) dihexafluorophosphate (**27**) as the negative electrode, poly(N-vinylcarbazole) or **PVK** as the positive electrode, and 1M *n*-Bu_4NPF_6 in propylene carbonate (PC) system as electrolyte (Figure 15).[59] The fully organic cell exhibited a theoretical specific capacity of about 100 $mAh/g_{(PVK)}$ with the intermediate potential difference of 1.8 V. A progressive decrease in the reversible capacity was noticed during the cycling due to a slight dissolution of the active materials in the electrolyte.

Poizot and coworkers provided another example of an all-organic anionic "rocking-chair" battery based on molecular viologen species **28**-**29** (Figure 15).[60] Incorporation of carboxylate functions to viologens has been demonstrated to limit their solubility in aprotic polar electrolytes. In lithium half-cells, both compounds exhibit two visible pseudo-plateaus are observed at ca. 2.4

and 1.9 V (*vs.* Li^+/Li) during the first reduction, corresponding to capacities of 130 and 110 mAh g^{-1} for **28** and **29**, respectively, quite close to the expected two-electron transfer. By coupling with dilithium 2,5-(dianilino)terephthalate (Li_2DAnT) as the positive electrode, the all-organic anionic rechargeable batteries based on crystalline host-electrode materials are capable of delivering a specific capacity of 27 mAh/g (electrodes) with a stable cycling over dozens of cycles (Figure 16). The same group further reported a complementary study by using a poorly soluble crosslinked polyviologen **30** as negative electrode.[61] Fully anionic batteries pairing Li_2DAnT with **30** were assembled giving rise to 0.7 V as output voltage with a specific capacity of 50 mAh per gram of Li_2DAnT.

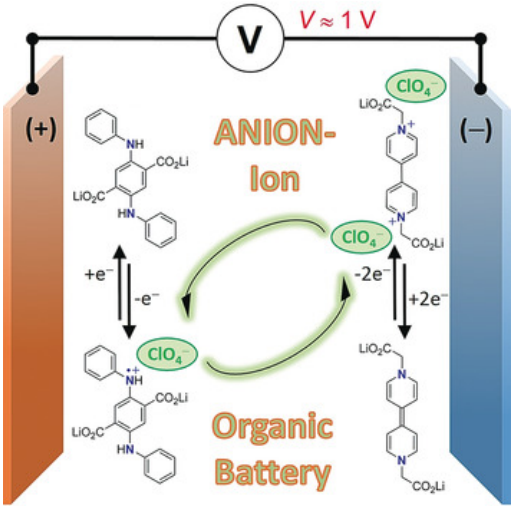

Figure 16. Conceptual illustration of the mechanism of the anion-shuttle battery based on **28** and **Li_2DAnT**. Reproduced with permission from Wiley, ref. 60.

In related work, Zhao and coworkers employed an insoluble polyxylylviologen chloride (**31**) as a chloride-ion storage electrode in chloride ion batteries (CIB) (Figure 15).[62] The battery was assembled in coin cells by using **31** as cathode, lithium metal anode, and 0.5 M

tributylmethylammonium chloride in propylene carbonate as electrolyte. The as-prepared **31** electrode exhibited a competitive discharge capacity of 140 mAh/g (86% of the theoretical discharge capacity). The incorporation of graphene in the **31** electrode leads to considerable enhancements in reversible capacity, cycling stability and rate capability, due to the increase of the electrical conductivity and charge transfer.

4. Carbonylpyridinium-based Electrodes for Li-ion Batteries

In 2019, Kang and coworkers exploited the NAD^+ motif for electrochemical energy storage in LOBs for the first time.[63] The capacity and operating voltage of **mNAD-X** (Figure 17) can be fine-tuned by altering the corresponding counter anion without modifying the redox center itself. Despite its lowest theoretical capacity, **mNAD-I** delivers the highest specific capacity of 77.7 mAh/g. This was attributed to the larger I^- anion providing the highest lithium-ion accessibility with sufficient free space, resulting in the highest lithium incorporation per **mNAD$^+$**. The delivered capacity of the various **mNAD-X** electrodes follows the order of $X^- = I^- > Br^- > Cl^-$. The redox potential was found to decrease with the size of the counter anion in the order of $Cl^- > Br^- > I^-$. This anion dependence of the voltage was tentatively explained by the hard–soft acid–base theory (HSAB theory). The hard acid Li^+ is likely exhibiting a stronger interaction with hard base Cl^-, leading to the highest stabilization energy for lithium insertion in **mNAD-Cl**, and thus the highest voltage. However, compared with conventional cathode materials, the cycle stability of **mNAD-X** electrode is still low and capacity deterioration after butyl-linking also remains a challenge in terms of energy density.

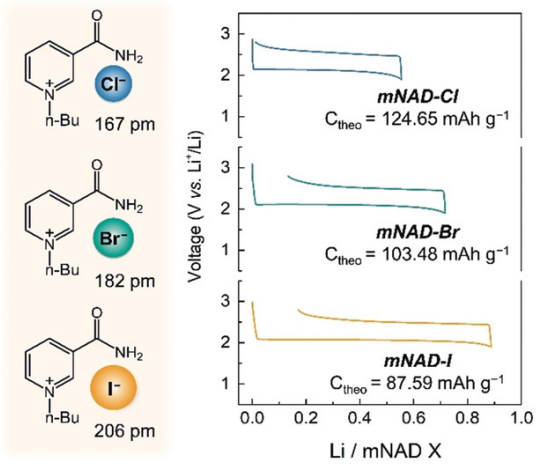

Figure 17. Electrochemical profile of ***m*NAD-X** with various halides. Reproduced with permission from Wiley, ref. 63.

To alleviate the undesired solubility in an electrode setting and to improve battery performance, our group reported the conjugated polymers **32-34** with pendant benzoyl-N-methylpyridinium (BMP) groups for LOBs in 2021 (Figure 18a).[64] The design strategy places the redox activity on spatially separated BMP units, so that the redox centers can operate relatively interference-free, while at the same time, providing an efficient electron-conduction pathway along the conjugated polymer backbone. Structural variations of the aromatic linker in the backbone have been demonstrated to exhibit a pronounced effect on the battery performance (**32** > **33** > **34**). At a current density of 0.2 A/g, the electrodes based on **32-34** exhibited stable capacities of 320, 300, and 260 mAh/g, respectively. Even at a relatively high current of 1 A/g, high specific capacities of up to 236 mAh/g can still be reached for **32** after 500 cycles. This, and the modest drop in capacity by 5-10% after 1000 cycles, support excellent cycle stability and great battery performance. The highest performance for **32** was attributed to its relatively lowest solubility, better conductivity, and introduction of the also redox-active benzothiadiazole as linker.[65] This

work provides the first example of redox-active conjugated polymers with bio-derived carbonylpyrinium for high-performance LOBs.

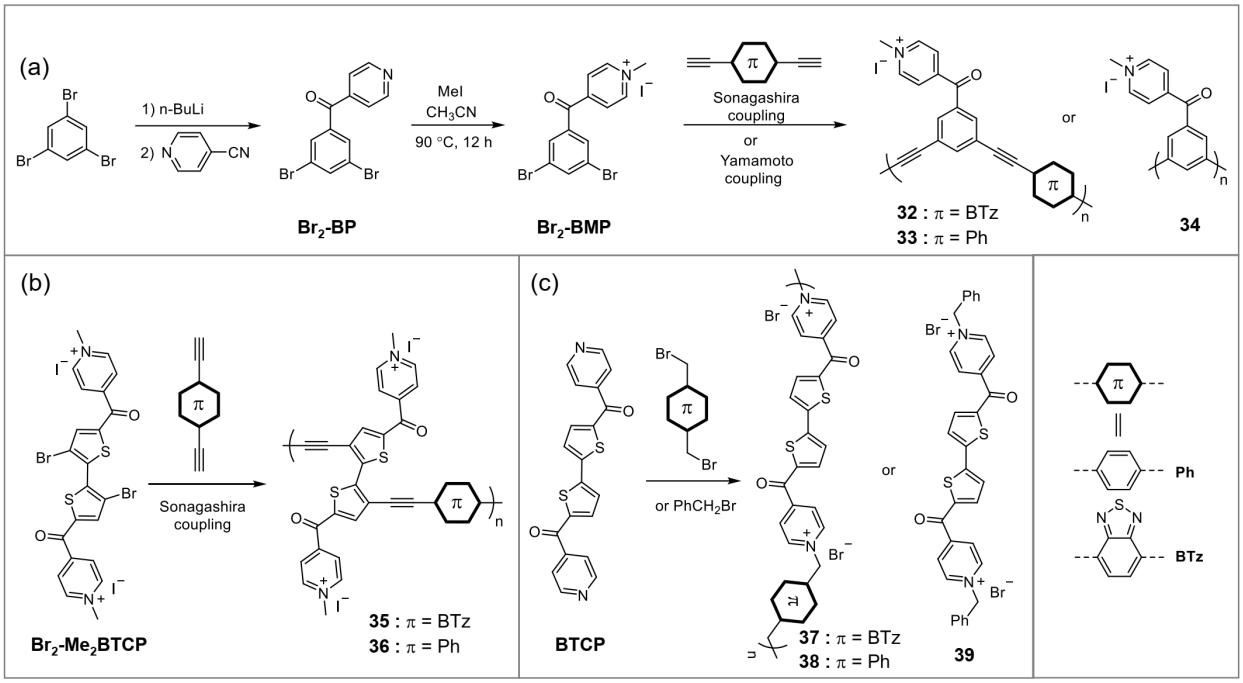

Figure 18. Synthesis of redox-active carbonylpyrinium incorporated polymers **32-34** (a), **35** and **36** (b), and **37-39** (c).

On the way to explore new acceptor scaffolds that can reversibly accept multiple electrons, we then developed two dicationic carbonylpyridinium-derivatives (**12** and **13**, Figure 3) that can reversibly store up to four electrons per molecule.[66] By extending the size of the π-conjugated core, their solubility is greatly reduced, compared to BMP, because of enhanced π-π stacking as well as their dicationic nature. Compound **13** with electron-donating bithienylene bridge helps to enhance the intramolecular charge transfer, leading to an improved electronic conductivity in the final battery device. Meanwhile, both cycling stability and rate performance are further enhanced through the incorporation of **13** into conjugated polymers **35** and **36** (Figure 18b). Impressively,

polymer **35** delivers not only the highest capacity but also the best cycling stability, reaching up to 574 mAh/g after 400 cycles at 0.5 A/g, and even as high as 807 mAh/g after 300 cycles at 0.2 A/g.

Similar to viologens, the nitrogen center of **BTCP** can easily be quaternized not only by MeI, but also benzyl bromide. Based on this strategy, we prepared the small-molecule model compound **39**, as well as two non-conjugated polymers (**37** and **38**) and exploited them for a range of alkali-ion (Li^+, Na^+ and K^+) batteries (Figure 18c).[67] Compared to the two conjugated relatives, the two non-conjugated polymers have high theoretical capacities (C_{theo} for **35**: 160 mAh/g, **36**: 137 mAh/g, **37**: 192 mAh/g, **38**: 167 mAh/g), due to the presence of lighter, electrochemically inactive groups. In a LOB half-cell setting, reversible capacities of 360 mAh/g (**37**), 190 mAh/g (**38**), and 80 mAh/g (**39**) were achieved after 300 cycles at 0.2 A/g. The trend **36** > **37** > **38**, further highlights the advantage of the polymer design and the judicious selection of the benzothiadiazole redox active linker. The experimental data also revealed that the insertion/extraction of the larger Na^+ and K^+ ions was much slower than that of Li^+, and the delivered capacity and cyclability of the **36** in sodium-ion and potassium-ion batteries were much lower than those in the lithium-ion-based relative.

Recently, our group also reported multi-electron acceptor materials **40a-f** by conjugation of naphthalenediimide (NDI) with two carbonylpyridinium units through a straightforward approach (Figure 19).[68] These positively charged skeletons can accept up to six electrons with excellent reversibility and stability, as demonstrated by CV and differential pulse voltammetry (DPV). For example, the first two reductions of **40a** (E^1 = -0.46 V, E^2 = -0.80 V, *vs*. Fc^+/Fc) are assigned to a two-electron uptake by the NDI scaffold and the following three redox couples (E^3 = -1.11 V, E^4 = -1.36 V, E^5 = -1.89 V) originate from the reduction of the carbonylpyridinium units. Compared to prototype **NDI-C8**, the reduction potentials of the NDI-carbonylpyridinium

conjugates underwent a significant positive shift by *ca.* 0.5-0.6 V. Such multiple redox systems are very rare, and each molecule can deliver 22/3 electrons by including Br^- counter anions. This attribute makes NDI-carbonylpyridinium conjugates particularly promising for high-density energy storage. Li-ion type organic batteries using **40d** as the cathode show a high specific capacity of 227.4 mAh/g (at 0.2 A/g), which is close to its theoretical value of 218 mAh/g.

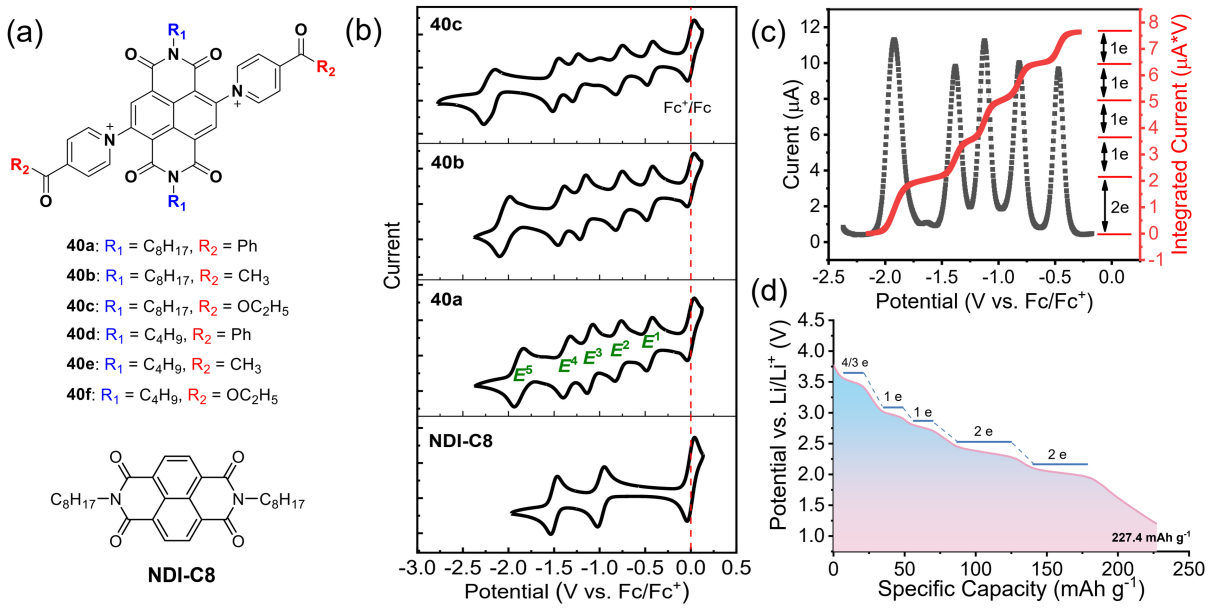

Figure 19. (a) Chemical structures of NDI-carbonylpyridinium conjugates. (b) CVs of and of **40a-c** and **NDI-C8** in DMF solution (c = 1 mM), with 0.1 M $TBAPF_6$ as the electrolyte. The scan rate of CV was 100 mV s^{-1}. (c) DPV on **40a** showing the current (black) and integrated current (red) for each reduction. (d) Galvanostatic charge-discharge profiles of **40d** at 0.2 A g^{-1}. Reproduced with permission from RSC, ref. 68.

5. Other Organic Solid-state Batteries beyond Li-ion

Rechargeable batteries based on multivalent cation carriers (e.g., Mg^{2+}, Zn^{2+}, Al^{3+}) are considered promising "post-lithium-ion" energy storage technologies, due to their high theoretical energy density, low cost, and intrinsic safety upon exposure to air and moisture. As a consequence of transferring two (or more) electrons per multivalent cation, they can theoretically provide higher

capacities than the traditional monovalent Li^+ cathodes while occupying a similar number of electroactive sites. Lu and coworkers showed the promising application of ethylviologen iodide (**EVI_2** or **16**) for high-rate and high-energy rechargeable Mg-ion batteries. The EV^{2+}/EV^0 redox couple demonstrates a superior rate performance (10 C) and stable cycle life (500 cycles) owing to intrinsic fast electrode kinetics. When coupling with two redox-active iodide anions, **EVI_2** achieved reversible four-electron storage with high energy density (304.2 Wh/kg) and stable cycle life (>100 cycles).[69]

Chen and coworkers reported a two-dimensional π-conjugated viologen-based organic framework (**41**) as organic host for multivalent cation (Zn^{2+}, Ca^{2+}) storage, and put forward an anion ligand-assisted intercalation pseudocapacitance mechanism (Figure 20).[70] During discharge, the viologen is reduced to its neutral form, and the released anions subsequently stabilize Zn^{2+} in the form of $[Zn^{2+}\cdot 2Cl^-\cdot 2H_2O]$ that preferentially adsorbs near the pyridine sites. Such near-surface intercalation pseudocapacitance enables fast kinetics with little structural change upon intercalation. It thus enables an excellent power density of 57 kW/kg over 20,000 cycles for Ca^{2+} storage and a power density of 14 kW/kg with a long cycling life over 45,000 cycles for Zn^{2+} storage. The work provides new insights into addressing the sluggish kinetics issues of multivalent cation storage in the electrodes design.

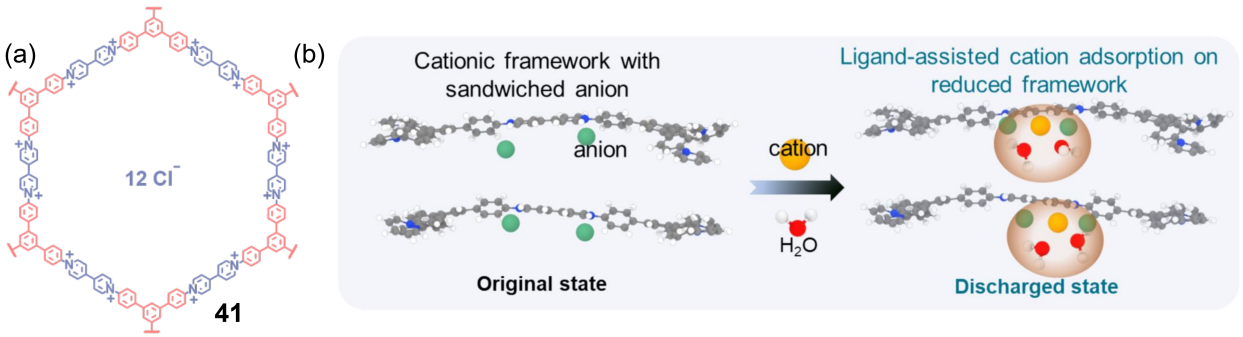

Figure 20. (a) Molecular structure of **41**. (b) Schematics of ligand-assisted multivalent cation intercalation process. Reproduced with permission from RSC, ref. 70.

6 Summary and Outlook

In summary, pyridinium species such as viologens and carbonylpyridiniums exhibit highly beneficial electrochemical properties (i.e., inherently reversible two-electron storage ability) that make both outstanding candidates for a range of electrochemical energy storage applications, including Li-ion type organic batteries (LOBs), that are the focus of this Spotlight. In addition, the chemistry of these fundamental building blocks is exceptionally versatile, allowing their structures to be tailored in a plethora of different ways to achieve a specific (additional) function without the loss of their beneficial electronic and/or redox properties. This includes the targeted modification of the carbon-based scaffold, as well as the embedded nitrogen centers. Judicious functionalization of the parent system was found to have significant impact on the overall electrochemical properties, by not only addressing the observed redox window, with direct implications for the achievable voltage in the final battery device, but also the number of electrons that can reversibly be stored within each building block, thereby directly impacting the energy storage density of the final device.

However, while modification of the scaffold can address important parameters for application as electrodes in a battery on the molecular scale, this may not translate into superior device performance in the end. A main reason for the observed shortcoming often lies within the drastically changing polarity of the electroactive species during reduction/oxidation (i.e., the charging/discharging cycles during battery operation), making them considerably soluble in the electrolyte solutions, and leading to rapid capacity fading. But suitable modification of the scaffold

can effectively address the issue by, for example, installing structural groups that enhance the supramolecular interaction with the other electrode composite materials, or incorporation into a polymer framework. The latter is particularly effective for viologens via the utilization of *N*-alkylation strategies. Importantly, this strategy commonly does not interfere with the electrochemical properties of the molecular scaffolds of the building blocks, and they can easily be retained in the bulk materials.

In addition, since both species are also inherently cationic in their native state, the presence of the required counter anions can also be effectively leveraged into additional energy-storage processes, as exemplified by the anion shuttle batteries that employ the redox chemistry of halides in addition to the energy storage capacity of the corresponding cationic pyridinium species.

All these beneficial features have led to many proof-of-concept studies to date that consider one or a combination of several of the mentioned elements in their materials design. These studies impressively showcase the exceptional versatility of viologen- and carbonylpyridinium-based materials and their utility as organic electrodes and have led to a rapid evolution of LOBs in recent years, whose performance now (almost) rivals that of the current state-of-the-art inorganic Li-ion batteries in terms of capacity, energy density, as well as longevity (Table 1).

Moreover, the latest representative developments with regard to battery types beyond Li-ion, such as Mg^{2+}, Zn^{2+}, Al^{3+}, provide important insights that pyridinium-based organics are also quite compatible with these multivalent ions as well, and given the high versatility from a chemical modification standpoint, the electrochemical and functional properties of the organic building blocks could be effectively tailored toward improved interplay with these multivalent ions, ultimately achieving optimal device performance as well.

Certainly, more work is required to develop these materials into true competitors, particularly since the inorganic Li-ion field continues to rapidly evolve as well. In addition, the organic batteries may not be equally applicable to all battery settings – i.e., large scale wind or solar energy storage *and* electric cars *and* handheld consumer electronics *and* other specialized applications – but they clearly have to potential to be used in at least one of these applications. The success of the modified viologen and carbonylpyridinium systems so far has shown that the future of organic batteries will be bright in either case.

Pyridinium species are just one example of successful organic building blocks for organic battery electrodes, and there is a growing pool of electroactive organic species that are already or may eventually be suitable for a similar practical use in batteries. We hope that this Spotlight has provided sufficient ideas to spark other researchers to design and/or discover further, new promising building blocks and develop them into equally powerful organic electrode materials.

Table 1. Summary of battery performance based on viologen and carbonylpyridinium electrodes.

Compounds	C_{thero} (mAh g^{-1})	Electrode composition	Capacity (mAh/g)/ [Current density]	Cycle Stability: Capacity (mAh/g) /Retention/Cycles/ Current density	Redox Window (V)	Counter electrode	Ref.
Viologen-based electrodes							
1	88	1: MWCNT: PVDF = 1:4:1	16 [1 C]	n.r.	1.8–3.2	Li	56
14a	97	14a: AB: PVDF = 4:5:1	70 [0.02 A/g]	38 / 54% / 10 / 0.02 A/g	1.2–3.5	Li	53
14b	96	14b: AB: PVDF = 4:5:1	67 [0.02 A/g]	10 / 15% / 10 / 0.02 A/g	1.2–3.5	Li	53
14c	81	14c: AB: PVDF = 4:5:1	55 [0.02 A/g]	10 / 18% / 10 / 0.02 A/g	1.2–3.5	Li	53
14d	97	14d: AB: PVDF = 4:5:1	65 [0.02 A/g]	47 / 72% / 10 / 0.02 A/g	1.2–3.5	Li	53
15	183	15: SP: PEO = 6:3:1	~240, ~125 [0.05, 0.1 A/g]	~80 / ~33% / 50 / 0.05 A/g	0.8–2.8	Li	54
16	229	16: SP: PVDF = 8:1:1	230, 210, 149 [0.1, 2, 5 C]	218 / 96% / 200 / 0.5C	1.6–4.0	Li	55
17	130	17: SP: PVDF = 8:1:1	130, 102 [0.1, 5C]	~110 / 98% / 200 / 0.5C	1.6–3.0	Li	55
16 (4e)	229	16: Vulcan carbon = 1:1	207 [1C]	200 / 96% /100 / 0.5C	0.5–3.0	Mg	73
16 (2e)	114	16: Vulcan carbon = 1:1	112, 91 [2, 10C]	~63 / 74% / 500 / 10C	0.5–2.5	Mg	73
18	71	18: MWCNT: PVDF = 1:4:1	31 [3 C]	n.r.	1.8–3.2	Li	56
19	107	19: SWCNT: PVDF = 4:4:2	32, ~26 [1/2, 1C]	~25 / ~96% / 120 / 1C	2.0–4.5	Li	57
21	53	21: SWCNT: PVDF = 4:8:3	~48 [1C]	53 / 110% / 500 / 1C	1.95–3.5	Li	58
22a	77	22a: CB: PVDF = 4:3:9	60, 40, 35, 26 [1/3, 1.5, 3, 8C]	60 / 82% / 70 / 1C	1.8–3.2	Li	56
22b	77	22b: CB: PVDF = 4:3:9	74, 61, 55, 44 [1/2, 2, 5, 10C]	40 / 84% / 150 / 1.5C	1.8–3.2	Li	56

23a	119	23a: CB: PVDF = 6:3:1	~580 [0.05 A/g]	416 / 57% / 40/ 0.1 A/g	0.001–3.0	Li	44
23b	108	23b: CB: PVDF = 6:3:1	~620 [0.05 A/g]	462 / 72% / 40 / 0.1 A/g	0.001–3.0	Li	44
23c	98	23c: CB: PVDF = 6:3:1	799, 684, 567, 463, 366, 252 [0.05, 0.1, 0.2, 0.5, 1, 2 A/g]	502 / 73% / 40 / 0.1 A/g	0.001–3.0	Li	44
24a	90	24a: KB: PVDF = 5:4:1	108, 84 [0.02, 1 A/g]	94 / 87% / 100 / 0.1 A/g	1.2–3.8	Li	59
24b	193	24b: KB: PVDF = 5:4:1	186, 157, 145, 133, 103, 77 [0.02, 0.04, 0.1, 0.2, 0.4, 1 A/g]	~125 / 74% / 100 / 0.1 A/g	1.2–3.8	Li	59
24c	193	24c: KB: PVDF = 5:4:1	~175, ~148, ~138, ~127, ~118, ~85 [0.02, 0.04, 0.1, 0.2, 0.4, 1 A/g]	~115 / 71% / 100 / 0.1 A/g	1.2–3.8	Li	59
25	77	25: CB: PVDF = 6:3:1	299, 219, 160, 112, 79, 54 [0.05, 0.1, 0.2, 0.4, 0.8, 1.6 A/g]	105 / 28% / 1000 / 0.8 A/g	0.005–3.0	Li	62
26	56	26: CB: PVDF = 6:3:1	554, 360, 278, 212, 164, 127 [0.05, 0.1, 0.2, 0.4, 0.8, 1.6 A/g]	359 / 100% / 1000 / 0.8 A/g	0.005–3.0	Li	62
41	124	41: KB: CMC = 5:4:1	~91, 80, 82 [0.5, 10, 20 A/g]	111 / 60% / 30600 / 0.5 A/g	0.4–1.4	Zn	74
41	124	41: KB: CMC = 5:4:1	~65, 41, 32 [0.5, 10, 20 A/g]	87 / 88% / 18000 / 0.5 A/g	2.1–4.2	Ca	74
Carbonylpyridium-based electrodes							
*m*NAD-Cl	125	*m*NAD-Cl: SP: PTFE = 4:4:2	~69 [0.05 A/g]	n.r.	1.9–2.8	Li	67
*m*NAD-Br	103	*m*NAD-Br: SP: PTFE = 4:4:2	~74 [0.05 A/g]	n.r.	1.9–2.8	Li	67
*m*NAD-I	88	*m*NAD-I: SP: PTFE = 4:4:2	78 [0.05 A/g]	n.r.	1.9–2.8	Li	67
11	165	11: CB: PVDF = 6:3:1	220, 150, 110, 77, 45 [0.2, 0.5, 1, 2, 5 A/g]	58 / 27% / 400 / 0.5 A/g	0.05–3.0	Li	70
12	165	12: CB: PVDF = 6:3:1	350, 230, 160, 110, 70 [0.2, 0.5, 1, 2, 5 A/g]	136 / 42% / 400 / 0.5 A/g 161 / 38% / 300 / 0.2 A/g	0.05–3.0	Li	70
13	162	13: CB: PVDF = 6:3:1	520, 350, 260, 180, 115 [0.2, 0.5, 1, 2, 5 A/g]	253 / 52% / 400 / 0.5 A/g 542 / 88% / 300 / 0.2 A/g	0.05–3.0	Li	70
32	159	32: CB: PVDF = 6:3:1	320, 250, 180, 140, 100 [0.2, 0.5, 1, 2, 5 A/g]	236 / 91% / 1000 / 1 A/g	0.005–3.0	Li	68
33	120	33: CB: PVDF = 6:3:1	300, 210, 150, 120, 90 [0.2, 0.5, 1, 2, 5 A/g]	200 / 75% / 1000 / 1 A/g	0.005–3.0	Li	68
34	166	34: CB: PVDF = 6:3:1	260, 180, 125, 90, 60	110 / 82% / 1000 / 1 A/g	0.005–3.0	Li	68

			[0.2, 0.5, 1, 2, 5 A/g]				
35	160	35: CB: PVDF = 6:3:1	520, 440, 365, 300, 230 [0.2, 0.5, 1, 2, 5 A/g]	574 / 95% / 400 / 0.5 A/g 807 / 127% / 300 / 0.2 A/g	0.05–3.0	Li	70
36	137	36: CB: PVDF = 6:3:1	360, 290, 230, 190, 145 [0.2, 0.5, 1, 2, 5 A/g]	316 / 70% / 400 / 0.5 A/g 317 / 65% / 300 / 0.2 A/g	0.05–3.0	Li	70
37	192	37: KB: PVDF = 6:3:1	610, 454, 361, 288, 204 [0.2, 0.5, 1, 2, 5 A/g]	360 / 44% / 300 / 0.2 A/g	0.005–3.0	Li	71
37	192	37: KB: PVDF = 6:3:1	230, 145, 105, 69, 44 [0.1, 0.2, 0.5, 1, 2 A/g]	210 / 51% / 100 / 0.1 A/g	0.005–3.0	Na	71
37	192	37: KB: PVDF = 6:3:1	163, 98, 76, 50, 33 [0.1, 0.2, 0.5, 1, 2 A/g]	91 / 27% / 100 / 0.1 A/g	0.005–3.0	K	71
38	167	38: KB: PVDF = 6:3:1	382, 241, 176, 131, 87 [0.2, 0.5, 1, 2, 5 A/g]	190 / 33% / 300 / 0.2 A/g	0.005–3.0	Li	71
39	149	39: KB: PVDF = 6:3:1	251, 161, 119, 84, 57 [0.2, 0.5, 1, 2, 5 A/g]	80 / 16% / 300 / 0.2 A/g	0.005–3.0	Li	71
40d	218	40d: CB: PVDF = 5:4:1	227 [0.2 A/g]	227 / 100% / 3500 / 1 A/g	1.2–3.8	Li	72

Theoretical capacity (C_{thero}) is calculated with the formula $C_{thero} = nF/3.6M_w$, n stands for the transferred electron number, F stands for Faraday constant, and M_w stands for molecular weight. **Carbon additives:** CB is carbon black; AB is acetylene black; KB is ketjen black; SP is super P; SWCNT is single-walled carbon nanotubes; MWCNT is multiwalled carbon nanotubes. **Binder additives:** PVDF is polytetrafluoroethylene; PEO is polyethylene oxide; PTFE is polytetrafluoroethylene; CMC is carboxymethyl cellulose. **n.r.** denotes a value not reported.

AUTHOR INFORMATION

Corresponding Authors

Xiaoming He - Key Laboratory of Applied Surface and Colloid Chemistry (Ministry of Education), School of Chemistry and Chemical Engineering, Shaanxi Normal University, Xi'an 710119, P.R. China; orcid.org/0000-0003-2596-7042; Email: xmhe@snnu.edu.cn

Thomas Baumgartner - Department of Chemistry, York University, 4700 Keele Street, Toronto, Ontario M3J 1P3, Canada; orcid.org/0000-0001-8066-0559; Email: tbaumgar@yorku.ca

Author Contributions

The manuscript was written through contributions of all authors. All authors have given approval to the final version of the manuscript.

Notes

The authors declare no competing financial interest.

Acknowledgment

The work from our groups highlighted herein was supported by the Fundamental Research Funds for the Central Universities National (GK202201006), the Innovation Capability Support Program of Shaanxi (No. 2020TD024), the Natural Sciences and Engineering Research Council of Canada, and the Canada Foundation for Innovation. X. H. thanks Shaanxi Normal University for the funding support. T. B. thanks Canada Research Chairs program.

References

(1) Cho, J.; Jeong, S.; Kim, Y. Commercial and Research Battery Technologies for Rlectrical Energy Storage Applications. *Prog. Energy Combust. Sci.* **2015**, *48*, 84-101.

(2) Placke, T.; Heckmann, A.; Schmuch, R.; Meister, P.; Beltrop, K.; Winter, M. Perspective on Performance, Cost, and Technical Challenges for Practical Dual-Ion Batteries. *Joule* **2018**, *2*, 2528-2550.

(3) Yu, X.; Manthiram, A. Sustainable Battery Materials for Next-Generation Electrical Energy Storage. *Adv. Energy Sustainability Res.* **2021**, *2*, 2000102.

(4) Armaroli, N.; Balzani, V. Solar Electricity and Solar Fuels: Status and Perspectives in the Context of the Energy Transition. *Chem. Eur. J.* **2016**, *22*, 32-57.

(5) Li, M.; Lu, J.; Chen, Z.; Amine, K. 30 Years of Lithium-Ion Batteries. *Adv. Mater.* **2018**, *30*, 1800561.

(6) Tian, Y.; Zeng, G.; Rutt, A.; Shi, T.; Kim, H.; Wang, J.; Koettgen, J.; Sun, Y.; Ouyang, B.; Chen, T.; Lun, Z.; Rong, Z.; Persson, K.; Ceder, G. Promises and Challenges of Next-Generation "Beyond Li-ion" Batteries for Electric Vehicles and Grid Decarbonization. *Chem. Rev.* **2021**, *121*, 1623-1669.

(7) Ponrouch, A.; Bitenc, J.; Dominko, R.; Lindahl, N.; Johansson, P.; Palacin, M. R. Multivalent Rechargeable Batteries. *Energy Stor. Mater.* **2019**, *20*, 253-262.

(8) Nayak, P. K.; Yang, L.; Brehm, W.; Adelhelm, P. From Lithium-Ion to Sodium-Ion Batteries: Advantages, Challenges, and Surprises. *Angew. Chem. Int. Ed.* **2018**, *57*, 102-120.

(9) Lei, X.; Liang, X.; Yang, R.; Zhang, F.; Wang, C.; Lee, C.-S.; Tang, Y. Rational Design Strategy of Novel Energy Storage Systems: Toward High-Performance Rechargeable Magnesium Batteries. *Small* **2022**, *18*, 2200418.

(10) Li, Z.; Tan, J.; Wang, Y.; Gao, C.; Wang, Y.; Ye, M.; Shen, J. Building Better Aqueous Zn-organic Batteries. *Energy Environ. Sci.* **2023**, *16*, 2398-2431.

(11) Faegh, E.; Ng, B.; Hayman, D.; Mustain, W. E. Practical Assessment of the Performance of Aluminium Battery Technologies. *Nature Energy* **2021**, *6*, 21-29.

(12) Li, T.; Bai, X.; Gulzar, U.; Bai, Y.-J.; Capiglia, C.; Deng, W.; Zhou, X.; Liu, Z.; Feng, Z.; Proietti Zaccaria, R. A Comprehensive Understanding of Lithium–Sulfur Battery Technology. *Adv. Funct. Mater.* **2019**, *29*, 1901730.

(13) Feng, K.; Li, M.; Liu, W.; Kashkooli, A. G.; Xiao, X.; Cai, M.; Chen, Z. Silicon-Based Anodes for Lithium-Ion Batteries: From Fundamentals to Practical Applications. *Small* **2018**, *14*, 1702737.

(14) Wang, H.; Yang, Y.; Guo, L. Nature-Inspired Electrochemical Energy-Storage Materials and Devices. *Adv. Energy Mater.*. **2017**, *7*, 1601709.

(15) Poizot, P.; Gaubicher, J.; Renault, S.; Dubois, L.; Liang, Y.; Yao, Y. Opportunities and Challenges for Organic Electrodes in Electrochemical Energy Storage. *Chem. Rev.* **2020**, *120*, 6490-6557.

(16) Schon, T. B.; McAllister, B. T.; Li, P.-F.; Seferos, D. S. The Rise of Organic Electrode Materials for Energy Storage. *Chem. Soc. Rev.* **2016**, *45*, 6345-6404.

(17) Kye, H.; Kang, Y.; Jang, D.; Kwon, J. E.; Kim, B.-G. p-Type Redox-Active Organic Electrode

Materials for Next-Generation Rechargeable Batteries. *Adv. Energy Sustain. Res.* **2022**, *3*, 2200030.

(18) Striepe, L.; Baumgartner, T. Viologens and Their Application as Functional Materials. *Chem. Eur. J.* **2017**, *23*, 16924-16940.

(19) Kathiresan, M.; Ambrose, B.; Angulakshmi, N.; Mathew, D. E.; Sujatha, D.; Stephan, A. M. Viologens: A Versatile Organic Molecule for Energy Storage Applications. *J. Mater. Chem. A* **2021**, *9*, 27215-27233.

(20) Zhang, P.; Li, M.; Yang, B.; Fang, Y.; Jiang, X.; Veith, G. M.; Sun, X.-G.; Dai, S. Polymerized Ionic Networks with High Charge Density: Quasi-Solid Electrolytes in Lithium-Metal Batteries. *Adv. Mater.* **2015**, *27*, 8088-8094.

(21) Evanko, B.; Yoo, S. J.; Chun, S.-E.; Wang, X.; Ji, X.; Boettcher, S. W.; Stucky, G. D. Efficient Charge Storage in Dual-Redox Electrochemical Capacitors through Reversible Counterion-Induced Solid Complexation. *J. Am. Chem. Soc.* **2016**, *138*, 9373-9376.

(22) Luo, H.; Wang, G.; Lu, J.; Zhuang, L.; Xiao, L. Viologen/Bromide Dual-Redox Electrochemical Capacitor with Two-Electron Reduction of Viologen. *ACS Appl. Mater. Interfaces* **2019**, *11*, 41215-41221.

(23) Striepe, L.; Vespa, M.; Baumgartner, T. Synthesis and Properties of Electron Accepting Star-Shaped Phosphaviologen Oligomers. *Org. Chem. Front.* **2017**, *4*, 717-723.

(24) Stolar, M.; Borau-Garcia, J.; Toonen, M.; Baumgartner, T. Synthesis and Tunability of Highly Electron-Accepting, N-Benzylated "Phosphaviologens". *J. Am. Chem. Soc.* **2015**, *137*, 3366-3371.

(25) Reus, C.; Stolar, M.; Vanderkley, J.; Nebauer, J.; Baumgartner, T. A Convenient N-Arylation Route for Electron-Deficient Pyridines: The Case of π-Extended Electrochromic Phosphaviologens. *J. Am. Chem. Soc.* **2015**, *137*, 11710-11717.

(26) Li, G.; Xu, L.; Zhang, W.; Zhou, K.; Ding, Y.; Liu, F.; He, X.; He, G. Narrow-Bandgap Chalcogenoviologens for Electrochromism and Visible-Light-Driven Hydrogen Evolution. *Angew. Chem. Int. Ed.* **2018**, *57*, 4897-4901.

(27) Madasamy, K.; Velayutham, D.; Suryanarayanan, V.; Kathiresan, M.; Ho, K.-C. Viologen-Based Electrochromic Materials and Devices. *J. Mater. Chem. C* **2019**, *7*, 4622-4637.

(28) Leventis, N.; Rawaswdeh, A.-M. M.; Zhang, G.; Elder, I. A.; Sotiriou-Leventis, C. Tuning the Redox Chemistry of 4-Benzoyl-N-methylpyridinium Cations through Para Substitution. Hammett Linear Free Energy Relationships and the Relative Aptitude of the Two-Electron Reduced Forms for H-Bonding. *J. Org. Chem.* **2002**, *67*, 7501-7510.

(29) Leventis, N.; Elder, I. A.; Gao, X.; Bohannan, E. W.; Sotiriou-Leventis, C.; Rawashdeh, A. M. M.; Overschmidt, T. J.; Gaston, K. R. The Redox Chemistry of 4-Benzoyl-N-methylpyridinium Cations in Acetonitrile with and without Proton Donors: The Role of Hydrogen Bonding. *J. Phys. Chem. B* **2001**, *105*, 3663-3674.

(30) Sevov, C. S.; Brooner, R. E. M.; Chénard, E.; Assary, R. S.; Moore, J. S.; Rodríguez-López, J.; Sanford, M. S. Evolutionary Design of Low Molecular Weight Organic Anolyte Materials for Applications in Nonaqueous Redox Flow Batteries. *J. Am. Chem. Soc.* **2015**, *137*, 14465-14472.

(31) Sevov, C. S.; Hendriks, K. H.; Sanford, M. S. Low-Potential Pyridinium Anolyte for Aqueous Redox Flow Batteries. *J. Phys. Chem. C* **2017**, *121*, 24376-24380.

(32) Hendriks, K. H.; Sevov, C. S.; Cook, M. E.; Sanford, M. S. Multielectron Cycling of a Low-Potential Anolyte in Alkali Metal Electrolytes for Nonaqueous Redox Flow Batteries. *ACS Energy Lett.* **2017**, *2*, 2430-2435.

(33) Shrestha, A.; Hendriks, K. H.; Sigman, M. S.; Minteer, S. D.; Sanford, M. S. Realization of an Asymmetric Non-Aqueous Redox Flow Battery through Molecular Design to Minimize Active Species Crossover and Decomposition. *Chem. Eur. J.* **2020**, *26*, 5369-5373.

(34) Sevov, C. S.; Hickey, D. P.; Cook, M. E.; Robinson, S. G.; Barnett, S.; Minteer, S. D.; Sigman, M. S.; Sanford, M. S. Physical Organic Approach to Persistent, Cyclable, Low-Potential Electrolytes for Flow Battery Applications. *J Am. Chem. Soc.* **2017**, *139*, 2924-2927.

(35) Janoschka, T.; Martin, N.; Martin, U.; Friebe, C.; Morgenstern, S.; Hiller, H.; Hager, M. D.; Schubert, U. S. An Aqueous, Polymer-Based Redox-Flow Battery Using Non-Corrosive, Safe, and Low-Cost Materials. *Nature* **2015**, *527*, 78-81.

(36) Janoschka, T.; Martin, N.; Hager, M. D.; Schubert, U. S. An Aqueous Redox-Flow Battery with High Capacity and Power: The TEMPTMA/MV System. *Angew. Chem. Int. Ed.* **2016**, *55*, 14427-14430.

(37) Yang, C. S.; Wang, Y. Y.; Wan, C. C. Electrochemical Kinetics of the Reduction of Methylpyridinium Salts. *J. Electrochem. Soc.* **1989**, *136*, 2592.

(38) Benniston, A. C.; Harriman, A.; Li, P.; Rostron, J. P. Controlling Electron Delocalisation in Constrained *N*,*N*′-Dimethyl-4,4′-Bipyridinium Dications. *Tetrahedron Lett.* **2005**, *46*, 7291-7293.

(39) Durben, S.; Baumgartner, T. 3,7-Diazadibenzophosphole Oxide: A Phosphorus-Bridged Viologen Analogue with Significantly Lowered Reduction Threshold. *Angew. Chem. Int. Ed.* **2011**, *50*, 7948-7952.

(40) Li, G.; Zhang, B.; Wang, J.; Zhao, H.; Ma, W.; Xu, L.; Zhang, W.; Zhou, K.; Du, Y.; He, G. Electrochromic Poly(chalcogenoviologen)s as Anode Materials for High-Performance Organic Radical Lithium-Ion Batteries. *Angew. Chem. Int. Ed.* **2019**, *58*, 8468-8473.

(41) Benniston, A. C.; Hagon, J.; He, X.; Yang, S.; Harrington, R. W. Spring Open Two-plus-Two Electron Storage in a Disulfide-Strapped Methyl Viologen Derivative. *Org. Lett.* **2012**, *14*, 506-509.

(42) Woodward, A. N.; Kolesar, J. M.; Hall, S. R.; Saleh, N.-A.; Jones, D. S.; Walter, M. G. Thiazolothiazole Fluorophores Exhibiting Strong Fluorescence and Viologen-Like Reversible Electrochromism. *J. Am. Chem. Soc.* **2017**, *139*, 8467-8473.

(43) Pan, M.; Lu, Y.; Lu, S.; Yu, B.; Wei, J.; Liu, Y.; Jin, Z. The Dual Role of Bridging Phenylene in an Extended Bipyridine System for High-Voltage and Stable Two-Electron Storage in Redox Flow Batteries. *ACS Appl. Mater. Interfaces* **2021**, *13*, 44174-44183.

(44) Demay-Drouhard, P.; Baumgartner, T. Highly Luminescent 4-Pyridyl-Extended Dithieno[3,2-b:2′,3′-d]phospholes. *J. Org. Chem.* **2020**, *85*, 14627-14633.

(45) Hu, S.; Li, T.; Huang, M.; Huang, J.; Li, W.; Wang, L.; Chen, Z.; Fu, Z.; Li, X.; Liang, Z. Phenylene-Bridged Bispyridinium with High Capacity and Stability for Aqueous Flow Batteries. *Adv. Mater.* **2021**, *33*, 2005839.

(46) Das, G.; Skorjanc, T.; Sharma, S. K.; Gándara, F.; Lusi, M.; Shankar Rao, D. S.; Vimala, S.; Krishna Prasad, S.; Raya, J.; Han, D. S.; Jagannathan, R.; Olsen, J.-C.; Trabolsi, A. Viologen-Based Conjugated Covalent Organic Networks via Zincke Reaction. *J. Am. Chem. Soc.* **2017**, *139*, 9558-9565.

(47) Kato, M.; Sano, H.; Kiyobayashi, T.; Yao, M. Viologen Derivatives Extended with Aromatic Rings Acting as Negative Electrode Materials for Use in Rechargeable Molecular Ion Batteries. *ChemSusChem* **2020**, *13*, 2379-2385.

(48) Ghosh, A.; Mitra, S. Facile Synthesis of Viologen and its Reversible Lithium Storage Property in Organic Lithium-Ion Batteries. *RSC Adv.* **2015**, *5*, 105632-105635.

(49) Ma, T.; Liu, L.; Wang, J.; Lu, Y.; Chen, J. Charge Storage Mechanism and Structural Evolution of Viologen Crystals as the Cathode of Lithium Batteries. *Angew. Chem. Int. Ed.* **2020**, *59*, 11533-11539.

(50) Stolar, M.; Reus, C.; Baumgartner, T. Xylene-Bridged Phosphaviologen Oligomers and Polymers as High-Performance Electrode-Modifiers for Li-Ion Batteries. *Adv. Energy Mater.* **2016**, *6*, 1600944.

(51) Bridges, C. R.; Borys, A. M.; Béland, V. A.; Gaffen, J. R.; Baumgartner, T. Phosphoryl- and Phosphonium-Bridged Viologens as Stable Two- and Three-Electron Acceptors for Organic Electrodes. *Chem. Sci.* **2020**, *11*, 10483-10487.

(52) Bridges, C. R.; Stolar, M.; Baumgartner, T. Phosphaviologen-Based Pyrene-Carbon Nanotube Composites for Stable Battery Electrodes. *Batteries Supercaps* **2020**, *3*, 268-274.

(53) Wang, Z.; Duan, A.; Jin, W.; Huang, X.; Li, Y. Poly(viologen halide)s: Both Cationic Main-Chain and Counter Anions are Active for High-Performance Organic Cathodes. *J. Mater. Chem. A* **2022**, *10*, 10026-10032.

(54) Wang, Z.; Qi, Q.; Jin, W.; Zhao, X.; Huang, X.; Li, Y. Trapping Halogen Anions in Cationic Viologen Porous Organic Polymers for Highly Cycling-Stable Cathode Materials. *Small* **2023**, *n/a*, 2303430.

(55) Fang, Y.; Yu, X.-Y.; Lou, X. W. Nanostructured Electrode Materials for Advanced Sodium-Ion Batteries. *Matter* **2019**, *1*, 90-114.

(56) Wu, M.; Zhao, Y.; Zhao, R.; Zhu, J.; Liu, J.; Zhang, Y.; Li, C.; Ma, Y.; Zhang, H.; Chen, Y. Chemical Design for Both Molecular and Morphology Optimization toward High-Performance Lithium-Ion Batteries Cathode Material Based on Covalent Organic Framework. *Adv. Funct. Mater.* **2021**, *32*, 2107703.

(57) Chen, L.; Zhu, X.; Zhang, Y.; Gao, G.; Xue, W.; Zhang, S.; Wang, X.; Zhang, Q.; He, X. A Fibrous Thiazolothiazole-Bridged Viologen Polymer for High-Performance Lithium-Ion Batteries. *J. Mater. Chem. A* **2021**, *9*, 18506-18514.

(58) Montoto, E. C.; Nagarjuna, G.; Hui, J.; Burgess, M.; Sekerak, N. M.; Hernández-Burgos, K.; Wei, T.-S.; Kneer, M.; Grolman, J.; Cheng, K. J.; Lewis, J. A.; Moore, J. S.; Rodríguez-López, J. Redox Active Colloids as Discrete Energy Storage Carriers. *J. Am. Chem. Soc.* **2016**, *138*, 13230-13237.

(59) Yao, M.; Sano, H.; Ando, H.; Kiyobayashi, T. Molecular Ion Battery: A Rechargeable System Without Using any Elemental Ions as a Charge Carrier. *Sci. Rep.* **2015**, *5*, 10962.

(60) Jouhara, A.; Quarez, E.; Dolhem, F.; Armand, M.; Dupré, N.; Poizot, P. Tuning the Chemistry of Organonitrogen Compounds for Promoting All-Organic Anionic Rechargeable Batteries. *Angew. Chem. Int. Ed.* **2019**, *58*, 15680-15684.

(61) Cadiou, V.; Gaillot, A.-C.; Deunf, É.; Dolhem, F.; Dubois, L.; Gutel, T.; Poizot, P. Pairing Cross-Linked Polyviologen with Aromatic Amine Host Structure for Anion Shuttle Rechargeable Batteries. *ChemSusChem* **2020**, *13*, 2345-2353.

(62) Xia, T.; Zhu, T.; Miao, Y.; Zhao, X. Polyxylylviologen Chloride as an Organic Electrode Material for Efficient Reversible Chloride-Ion Storage. *ACS Appl. Energy Mater.* **2022**, *5*, 6980-6985.

(63) Kim, J.; Ko, S.; Noh, C.; Kim, H.; Lee, S.; Kim, D.; Park, H.; Kwon, G.; Son, G.; Ko, J. W.; Jung, Y.; Lee, D.; Park, C. B.; Kang, K. Biological Nicotinamide Cofactor as a Redox-Active Motif for Reversible Electrochemical Energy Storage. *Angew. Chem. Int. Ed.* **2019**, *58*, 16764-16769.

(64) Gao, G.; Wang, X.; Chen, L.; Baumgartner, T.; He, X. Conjugated Polymers with Benzoyl-N-methylpyridinium Units: An Effective Design Strategy for High-Performance Lithium-Ion Batteries. *Chem. Mater.* **2021**, *33*, 4596-4605.

(65) Chen, L.; Bridges, C. R.; Gao, G.; Baumgartner, T.; He, X. Poly(5-vinylbenzothiadiazole) for High-Performance Lithium-Ion Batteries. *ACS Appl. Energy Mater.* **2019**, *2*, 7315-7320.

(66) Wang, X.; Xue, W.; Gao, G.; Chen, L.; Baumgartner, T.; He, X. Bio-Derived 4-Electron-Accepting Carbonyl-N-Methylpyridinium Species for High-Performance Lithium-Organic Batteries. *Cell Rep. Phys. Sci.* **2022**, *3*, 100951.

(67) Wang, X.; Chen, L.; He, X. Bio-Inspired Non-Conjugated Poly(carbonylpyridinium) as Anode Material for High-Performance Alkali-ion (Li^+, Na^+, and K^+) Batteries. *J. Colloid Interface Sci.* **2023**, *643*, 541-550.

(68) Lin, Q.; Li, H.; Chen, L.; He, X. Naphthalenediimide-Carbonylpyridiniums: Stable Six Electron Acceptors for Organic Cathodes. *Mater. Chem. Front.* **2023**.

(69) Sun, Y.; Zou, Q.; Lu, Y.-C. Fast and Reversible Four-Electron Storage Enabled by Ethyl Viologen for Rechargeable Magnesium Batteries. *Adv. Energy Mater.* **2019**, *9*, 1903002.

(70) Xie, L.; Xu, K.; Sun, W.; Fan, Y.; Zhang, J.; Zhang, Y.; Zhang, H.; Chen, J.; Shen, Y.; Fu, F.; Kong, H.; Wu, G.; Wu, J.; Chen, L.; Chen, H. Localized Ligands Assist Ultrafast Multivalent-Cation Intercalation Pseudocapacitance. *Angew. Chem. Int. Ed.* **2023**, *62*, e202300372.

TOC Graphic